XI International Conference on Computational Methods in Marine Engineering

Sail-Induced Resistance Comparison for the KVLCC2 and the KCS

F. Bickert[1,*], L. Gentaz[1], S. Delvoye[2] and A. Babarit[1]

[1] Laboratoire de recherche en Hydrodynamique, Énergétique et Environnement Atmosphérique
UMR 6598, Nantes Université, École Centrale de Nantes, CNRS, Nantes, France
[2] Zéphyr Et Borée, Lorient, France
[*] florent.bickert@ec-nantes.fr

ABSTRACT

Wind propulsion is a promising way of decarbonasing the merchant fleet. The number of ships equipped with one or several wind propulsion systems has significantly increased in the recent years, with more than 60 ships equipped since 2010. Adding a wind-propulsion system on a merchant ship generates an aerodynamic propulsion force which is wanted, but also an additional aerodynamic side force. This side force is responsible for the creation of an added resistance, due to higher leeway and rudder angles, that can reduce the manoeuvrability as well as the course keeping ability (Kramer and Steen, 2022). This so-called sail-induced resistance must thus be evaluated to know the real benefits of the wind propulsion system and to avoid manoeuvrability issues. This study evaluates the sail-induced resistance for two ship geometries: KVLCC2 (320-meter-long tanker) and KCS (230-meter-long containership). The sail-induced resistance is computed by resolving the steady-state force balance of the ship, using the open-source performance prediction program `xWASP_CN` developed by Charlou et al. (2023). The 4 DOF MMG manoeuvring model (Okuda et al., 2023) is used because it has already been validated through model-scale free running tests for both ship geometries. First, a validation of the implementation of the MMG model in the performance prediction program is proposed by comparing simulated and experimental results of turning-circle manoeuvers for both ships. Then, the sail-induced resistance is computed for each ship by applying a side force which is proportional to the straight-ahead resistance of the ship. The results are made non-dimensional to ease the comparison between the two ships.

Keywords: wind propulsion, sail-induced resistance, KCS, KVLCC2, MMG manoeuvring

1 INTRODUCTION

Today, a variety of Wind Propulsion Systems (WPS) exists for cargo ships: classical soft sails, Flettner rotors, soft and hard wingsails, suction wings, kites etc. (Kolodziejski and Sosnowski, 2025). Under the action of wind, a WPS generates an aerodynamic force which has components along and perpendicular to the ship longitudinal axis: a thrust force and a side force, respectively. The side force makes the ship sail at an angle that is called the leeway (or drift) angle. In steady state, the WPS side force is compensated by the hull side force and the rudder side force. A challenge of wind-assisted ship propulsion is that these drift-induced hull and rudder side forces come at the cost of an additional resistance.

Kramer and Steen (2022) investigated the relationship between the WPS side force and the additional resistance, which they coined *sail-induced resistance*. They considered a 120 m tramper equipped with three wingsails on a Baltic route. They found that the average sail-induced resistance represents a significant 5% to 14% of the total resistance depending on the ship speed. It is the same order of magnitude as the wave-added resistance. Sail-induced resistance being a side effect of hull and rudder side forces generation, it is expected to be ship-dependent. The present study contributes to investigate this dependency by assessing the sail-induced resistance for two academic ships: the KVLCC2 and the KCS (Stern et al., 2011).

Moreover, for most WPS, the high vertical position of the point of application of the aerodynamic force is responsible for a large heeling moment. Tillig and Ringsberg (2020) pointed out the importance of considering heel for wind-powered ships, first to verify its impact on transverse stability but also because it modifies the aerodynamic force. The effect of heel was neglected in Kramer and Steen (2022) because of the high transverse stability of the ship they investigated. However, the heel is considered in the present study because the KCS has a low transverse stability.
The hydrodynamic side force is generated by the hull but also the rudder. The rudder side force is indeed necessary to compensate the yaw moment induced by the hull side force and the WPS side force. The larger the rudder side force, the larger the rudder angle. Kramer and Steen (2022) found that increasing the WPS side force increases the rudder angle. A too large rudder angle is an issue because it reduces the manoeuvring capabilities of the ship. Therefore, the rudder angle is also investigated in the present study.

2 METHODS

The method follows that introduced by Kramer and Steen (2022): a numerical ship model is used for which the WPS effect is modelled by a constant side force proportional to the straight-ahead resistance without WPS. The advantage of this method is that it is WPS-independent while allowing the sailing ability of several ships to be compared.
The numerical models of the KVLCC2 and KCS have been developed within the open-source software `xWASP_CN`[1] (Charlou et al., 2023), which enables steady-state motion to be computed. `xWASP_CN` relies on the temporal 6-DOF dynamic ship simulator `xdyn`[2].

2.1 `xdyn` Ship Simulator

`xdyn` is a 6 Degrees-Of-Freedom (DOF) solver based on Newton-Euler's laws of motion for a rigid body, using a system-approach modelling (Fossen, 2011). The ship position in the fixed frame $\mathcal{R}_0$ is denoted $\boldsymbol{X} = (x, y, z)$, her velocity projected in ship frame $\mathcal{R}_b$ is denoted $\boldsymbol{U} = (u, v, w)$, and her rotational velocity in ship frame is denoted $\Omega = (p, q, r)$. The rotations of the ship relative to the fixed frame are defined using the Cardan/Tait-Bryan convention. Roll, pitch and yaw angles are denoted ϕ, θ and ψ, respectively. In the following, the generalised position vector $\boldsymbol{X}_u = (x, y, z, \phi, \theta, \psi)$ and the generalised velocity vector $\boldsymbol{V}_u = (u, v, w, p, q, r)$ are used for convenience. The equation of motions reads:

$$(\mathbf{M} + \mathbf{M}_A)\dot{\boldsymbol{V}}_u + \mathbf{C}(\boldsymbol{V}_u)\boldsymbol{V}_u = \sum \boldsymbol{\tau}_{G,\mathcal{R}_b} \tag{1}$$

where $\mathbf{M}$ and $\mathbf{M}_A$ are the rigid-body mass matrix and the added mass matrix at the ship centre of gravity G, $\mathbf{C}(\boldsymbol{V}_u)$ corresponds to the Coriolis and centripetal matrix due to the rotation of $\mathcal{R}_b$ around $\mathcal{R}_0$ and $\sum \boldsymbol{\tau}_{G,\mathcal{R}_b}$ is the sum of the generalised external forces (except for the added mass forces). In system-approach modelling, the forces acting on a body are independently modelled as a function of $\boldsymbol{X}_u$ and $\boldsymbol{V}_u$ and the environmental conditions.

2.2 `xWASP_CN` Performance Prediction Program

`xWASP_CN` is a Performance Prediction Program for wind-powered ship. It performs dynamic simulations and solves the steady state for a certain set of wind and wave conditions, by launching `xdyn` requests. The steady state is the static equilibrium of forces when the ship is subject to steady environmental conditions. In steady state, Eq. 1 simplifies to:

$$\sum \boldsymbol{\tau}_{G,\mathcal{R}_b} = \mathbf{0} \tag{2}$$

[1] https://gitlab.com/lheea/xwasp_cn
[2] https://gitlab.com/sirehna_naval_group/sirehna/xdyn

Assuming a rectilinear motion of the ship in the horizontal plane, some of the states in $\boldsymbol{X}_u$ and $\boldsymbol{V}_u$ are null or fixed: $\Omega = \mathbf{0}$ (no rotational velocities), $\dot{z} = 0$ (no vertical velocity), $x = y = 0$ (arbitrary horizontal position), $\psi = 0$ (fixed course) and $\sqrt{\dot{x}+\dot{y}} = V$ (fixed Speed Over Ground V). The static equilibrium is solved using an in-house root-finding algorithm based on the assumption that the problem described by Eq. 2 is diagonal-dominant, which is usually the case for a ship. Under this assumption, each force or moment equation is mainly influenced by one of the unknowns, allowing to find a decoupled solution for each equation. The obtained decoupled solution is used as a starting point for the coupled root-finding procedure. A validation of this algorithm was performed for a 18-feet catamaran fitted wih a Flettner rotor (Charlou et al., 2023).

2.3 Forces

A number of force models are available in `xWASP_CN` and `xdyn` which can be activated depending on the modelling needs. In the case of performance prediction for wind-assisted ships in steady state, the following models are required: WPS force, hull force, propeller force and rudder force. Models for added wave resistance and windage may also be considered, although they are not taken into account in the present study.

2.3.1 Manoeuvring forces

The manoeuvring forces are the hydrodynamic forces applied on the hull ($\boldsymbol{F}_{\mathrm{H}}$), the rudder ($\boldsymbol{F}_{\mathrm{R}}$) and the propeller ($\boldsymbol{F}_{\mathrm{P}}$). A common model for the manoeuvring forces is that of the Mathematical Manoeuvring Group (MMG) in which the hull forces are expressed as a Taylor expansion of u, v and r while the rudder and the propeller forces are computed with dedicated submodels taking hull-rudder-propeller interactions into account. Yasukawa and Yoshimura (2014) provided a thorough explanation of the MMG model with 3 DOF as well as a validation case for the KVLCC2. The model was later extended to 4 DOF and a validation case for the KCS was given by Okuda et al. (2023). The MMG model depends on coefficients (which are called hydrodynamic coefficients) that can be obtained through regressions based on experimental or virtual captive tests. In the present study, the hydrodynamic coefficients are taken from Yasukawa and Yoshimura (2014) for the KVLCC2 and Okuda et al. (2023) for the KCS. In both cases, they were derived from experimental captive tests in a towing tank.

The MMG model was implemented as an external force in `xdyn`. Although only the static part of the model is needed for steady-state calculations, the entire dynamic model was implemented and then validated for consistency with the other force models and also for potential future uses.
The first validation case is a turning circle with the KVLCC2 at scale 1/45.7 with an initial speed $u(t = 0) = 1.180$ m/s (i.e. 15.5 kt at full scale), as presented by Yasukawa and Yoshimura (2014). The manoeuvrer is carried out with a rudder angle $\delta = \pm 35°$. To reproduce the 3 DOF simulation, sinkage, trim and roll are blocked using the method presented in Babarit and Charlou (2023). Figure 1a shows the trajectory obtained with `xdyn` as well as the *reference* experimental and *reference* simulated trajectories from Yasukawa and Yoshimura (2014). The trajectories from `xdyn` and from the reference simulation overlap very well for $\delta = -35°$, while for $\delta = +35°$ the turning radius is slightly smaller for the `xdyn` trajectory.
The second validation case is a turning circle with the KCS at scale 1/65.833 with an initial speed $u(t = 0) = 1.268$ m/s (i.e. 20 kt at full scale), as presented by Okuda et al. (2023). The 4 DOF simulation is performed by blocking sinkage and trim. Figure 1b shows the trajectory obtained with `xdyn` and the reference experimental and reference simulated trajectories from Okuda et al. (2023). The `xdyn` trajectory has a smaller turning radius than the reference simulated trajectory for both rudder angles, but is closer to the experimental trajectory at the beginning of the manoeuvrer. The differ-

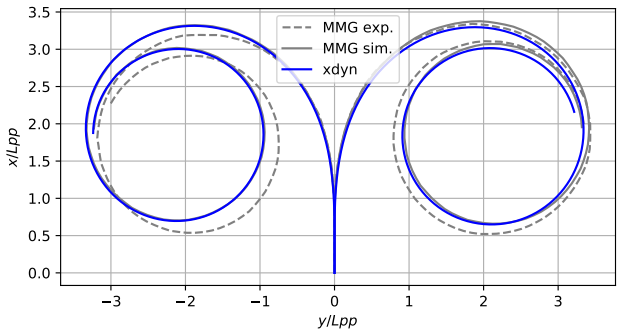

(a) KVLCC2 at scale 1/45.7 with an initial speed $u_0 = 1.180$ m/s (3 DOF).

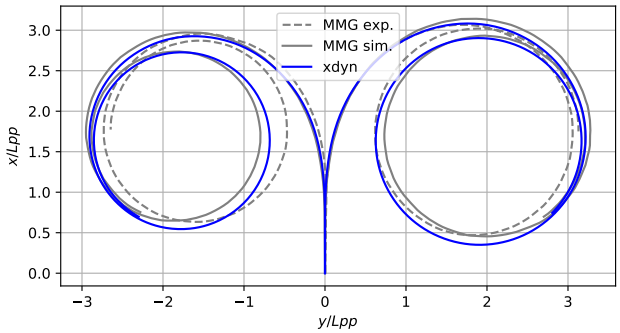

(b) KCS at scale 1/65.833 with an initial speed $u_0 = 1.268$ m/s (4 DOF).

Figure 1: Turning circle with $\delta = \pm 35°$. Blue: xdyn simulation. Grey: experimental (dashed line) and reference simulation (solid line) trajectories (Yasukawa and Yoshimura, 2014; Okuda et al., 2023).

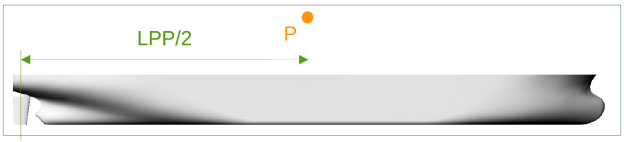

(a) Side view.

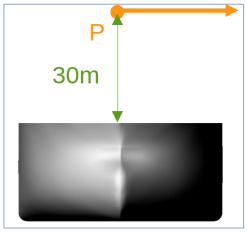

(b) Front view.

Figure 2: Point of application of the aerodynamic side force $F_{y,\mathrm{WPS}}$ in the case of the KVLCC2.

ences between the simulations may come from assumptions which we made for parameters of the MMG model not provided in Okuda et al. (2023), e.g. the straight-ahead resistance coefficient R'_0.

2.3.2 Aerodynamic forces

The ship is also subject to aerodynamic forces due to windage and the WPS. In the present study, the windage is neglected. The WPS force is modelled by a constant side force $\boldsymbol{F}_{\mathrm{WPS}}$ applied to a point P located at midship, 30m above the ship deck (Fig. 2). The coordinates of this force in ship frame $\mathcal{R}_b$ are $(0, F_{y,\mathrm{WPS}}, 0)$. Following Kramer and Steen (2022), we assume that $F_{y,\mathrm{WPS}}$ is proportional to R_0, the straight-ahead resistance when no side force is applied ($R_0 > 0$). The side force ratio s is introduced as:

$$s = \frac{F_{y,\mathrm{WPS}}}{R_0} \tag{3}$$

Kramer and Steen (2022) showed results for $s \in [0, 5]$. However, they found for their wind-propelled ship that the average value for s taking into account wind statistics on the route they investigated was between 0.6 and 1.4 depending on the ship speed. Thus, in the present study, only values of s between 0 and 2 are considered.

3 RESULTS

In this section, results are shown at full scale. The forward speed for the KVLCC2 is $V = 15.5$ kt while that of the KCS is $V = 20$ kt. The calm water resistance R_0 was Reynolds-scaled using the

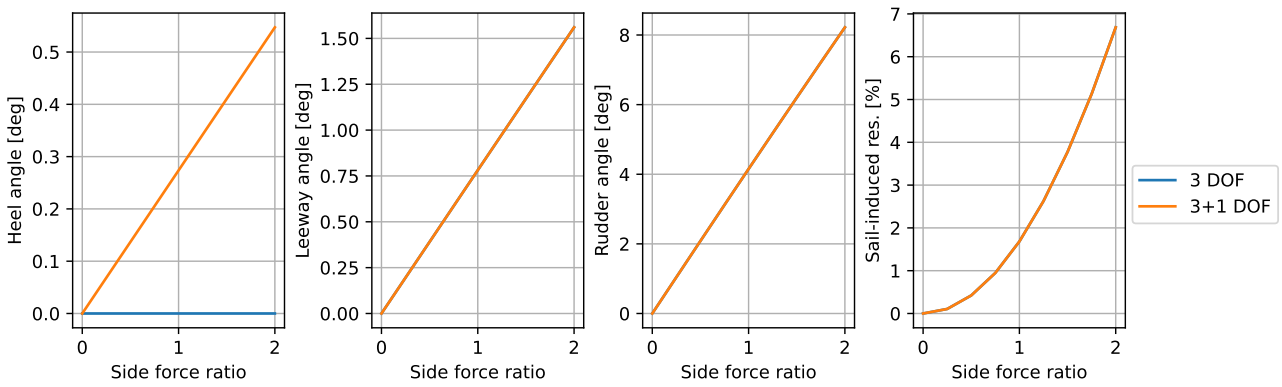

Figure 3: KVLCC2 response to an increasing aerodynamic side force at $V = 15.5$ kt.

usual ITTC78 extrapolation method (ITTC, 2014). The other hydrodynamic coefficients are the same at full scale and model scale, except for the KVLCC2 wake factor which changes from 0.40 at model scale to 0.35 at full scale, according to Yasukawa and Yoshimura (2014).

3.1 KVLCC2

For the KVLCC2, two cases are run: 3 DOF and 3+1 DOF. The 3+1 DOF approach is similar to the 3 DOF approach except that the heel angle is computed using the ship metacentric height (GM) without impacting the forces for the other motions. The 4 DOF case is not computed because no roll coefficients were found for this ship in the literature. Figure 3 shows the results of the 3 DOF and the 3+1 DOF simulations for the KVLCC2 at $V = 15$ kt. Heel angle, leeway angle, rudder angle and relative sail-induced resistance are plotted as a function of side force ratio s. The relative sail-induced resistance is defined as $\frac{R-R_0}{R_0}$, where R is the ship resistance with WPS ($R > 0$):

$$R = -(F_{x,H} + F_{x,R}) \tag{4}$$

As expected, apart from the heel angle, the results are the same either with 3DOF or with 3+1 DOF. Leeway angle, rudder angle and sail-induced resistance increase as side force ratio increases, as in Kramer and Steen (2022). The 3+1 DOF simulation gives very small heel angles, with a maximum of 0.5° for $s = 2$. The heel is therefore negligible, which justifies the use of a 3 DOF model instead of a 4 DOF model for this ship. The sail-induced resistance reaches 6.7% at $s = 2$, for a rudder angle of 8.2°.

The contributions of the hull and the rudder to the hydrodynamic side force and the sail-induced resistance are plotted in Fig. 4 for the 3+1 DOF case at $s = 2$. One can see that the rudder contributes to 47% of the hydrodynamic side force and 95% of the sail-induced resistance. This shows that the rudder is dramatically less efficient than the hull for generating side force.

3.2 KCS

For the KCS, three cases are investigated: 3 DOF, 3+1 DOF and 4 DOF. Figure 5 shows the results of the 3 DOF, 3+1 DOF and 4 DOF simulations for the KCS at $V = 20$ kt. One can notice slight differencies between 3 DOF and 3+1 DOF results for rudder angle, leeway angle and sail-induced resistance. These differences are caused by the projection of forces and velocities from ship frame $\mathcal{R}_b$ to fixed frame $\mathcal{R}_0$ due to large heel values. The heel values are indeed much larger than for the KVLCC2, reaching 15.2° at $s = 2$.

The rudder and leeway angles for the 3 DOF and the 3+1 DOF cases are similar to those obtained with the KVLCC2. The sail-induced resistance is a bit larger, reaching 10.0% for $s = 2$.

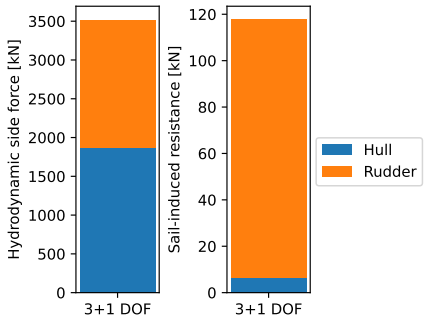

Figure 4: Forces distribution at $s = 2$ for the KVLCC2 at $V = 15.5$ kt.

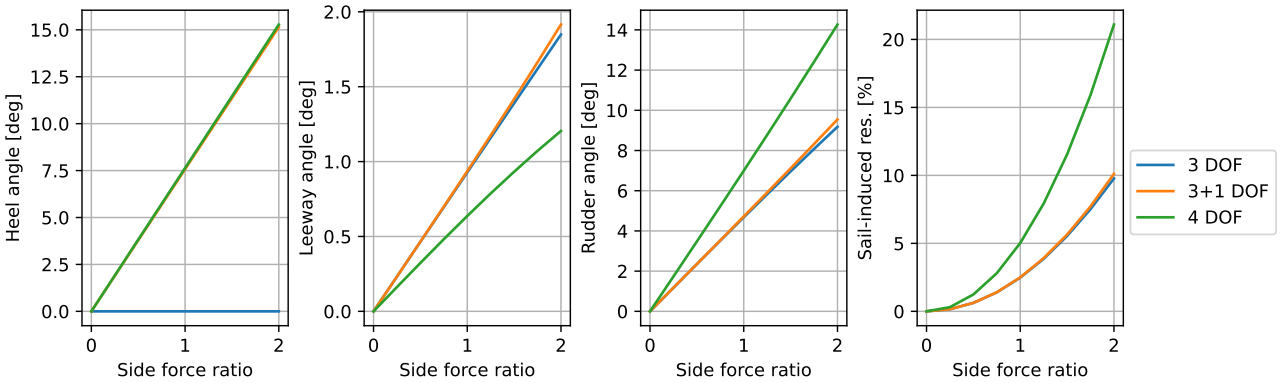

Figure 5: KCS response to an increasing aerodynamic side force at $V = 20$ kts.

With 4 DOF, the sail-induced resistance increases up to 21.1% for $s = 2$ while the rudder angle increases from 9.2° with 3 DOF to 14.3°. Only the leeway angle decreases from 1.8° to 1.2°. This indicates that in 4 DOF the rudder contribution to the transverse equilibrium increases while the hull contribution decreases.

The contributions of the hull and the rudder to the hydrodynamic side force and the sail-induced resistance are plotted on Fig. 6 for the 3+1 DOF and 4 DOF cases at $s = 2$. For the 3+1 DOF case, the rudder contributes to 45% of the hydrodynamic side force and 88% of the sail-induced resistance. For the 4 DOF case, the rudder contributes to 65% of the hydrodynamic side force and 92% of the sail-induced resistance. As for the KVLCC2, the rudder is less efficient than the hull for generating side force.

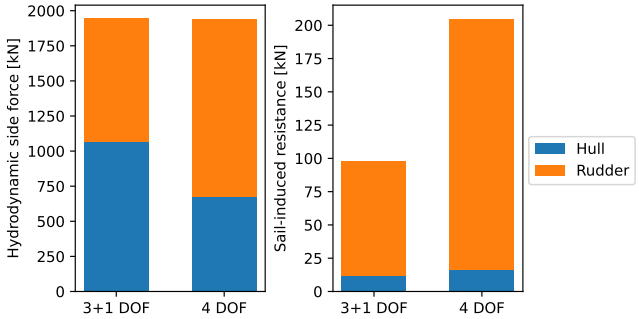

Figure 6: Forces distribution at $s = 2$ for the KCS at $V = 20$ kt.

4 CONCLUSIONS

In this study, we investigated the effect of hull shape on sail-induced resistance. The considered hull shapes are the well-known KVLCC2 and KCS. The effect of the WPS was modeled by a side force which is proportional to the straight-ahead resistance of the ship without WPS. The side force is increased up to twice the straight-ahead resistance. The simulations were performed for 3 DOF and 3+1 DOF for the KVLCC2 and 3 DOF, 3+1 DOF and 4 DOF for the KCS.
As expected, the sail-induced resistance increases as the WPS side force increases for both ships. However, the sail-induced resistance is found to be significantly smaller for the KVLCC2 than for the KCS: for s=2, it is 6.7% for the KVLCC2 at 15.5 kt but 21.1% for the KCS at 20 kt, whereas Kramer and Steen (2022) found 23% for a 120 m tramper at 12 kt. This shows that the hull shape has a significant effect on the sail-induced resistance. In addition, the rudder contribution to the sail-induced resistance was found to be greater than 90% for both ships whereas it is 73% in Kramer and Steen (2022). This demonstrates that the rudder is less efficient than the hull for generating an hydrodynamic side force. Note that the WPS force is kept at midship in this study, but the contribution of each force to side force and sail-induced resistance would be different if the WPS was longitudinally moved forward or backward on the ship deck.
The heel angle was found to be small ($< 0.6°$) for the KVLCC2. In contrast, it goes up to 15.2° for the KCS. Moreover, considering the heel or not has a large impact on sail-induced resistance for the KCS. Therefore, consideration should be given to the heel angle when evaluating sail-induced resistance.
Results also show that heel angle, leeway angle and rudder angle increase when side force increases. For the KVLCC2, the maximum heel angle is 0.5° and the maximum rudder angle is 8.2°, which is acceptable from an operational point of view. However, for the KCS, the heel angle reaches a maximum value of 15.2°, which is not operationnally acceptable. Note that it is very unlikely to have a wind-propelled ship sailing at 20 kt due to apparent wind generation: since the WPS side force is proportional to the forward speed resistance in this study, reducing the ship speed would decrease the heel angle. It is also found that the maximum rudder angle is 14.3° for the KCS. As a comparison, Alterskjær et al. (2024) defined a maximum steady-state rudder angle at 10° for the design of the new series of Norwegian Coastal Express, based on feedback from existing vessels. Although this threshold does not necessarily apply for a containership like the KCS, it is seen that the WPS has a huge impact on steering.

Improvements to the present work are to use weather statistics to get a more realistic value for the side force ratio, depending on the investigated WPS. Since the propeller speed will decrease when the WPS provides thrust, the flow velocity at the rudder location will reduce too, resulting in smaller rudder forces: this should also be evaluated. The impact of the WPS longitudinal position on the static equilibrium could also be studied.
A natural solution to reduce sail-induced resistance and rudder angle is to use hydrodynamic appendages. Several types of appendages have already been studied: small-aspect-ratio appendages such as bilge keels (van der Kolk et al., 2021); high-aspect-ratio appendages such as a central keel (Kramer and Steen, 2022) or diagonal foils (Marimon Giovannetti et al., 2021). Future work will investigate the impact of adding such appendages to reduce both the rudder angle and the sail-induced resistance.

ACKNOWLEDGEMENTS

The authors gratefully acknowledge the financial support of the French Public Investment Bank through the Mervent 2025 project allocated to Centrale Nantes, France.

REFERENCES

A. Alterskjær, A. Bruyat, A. Östman, J. Dæhlen, T. Mak, T. Skjong, A. Rødland, and G. Christiansen. Wind propulsion for Hurtigruten's future zero emission cruise vessels (project Sea Zero). In *Wind Propulsion 2024*, pages 1–17. Royal Institution of Naval Architects, Oct. 2024.

A. Babarit and M. Charlou. A Method for Forcing a Number of Motions or Rotations in 6 Degrees of Freedom Ship Simulators. *Journal of Sailing Technology*, 8(01):255–275, Dec. 2023. ISSN 2475-370X. doi: 10.5957/jst/2023.8.13.255.

M. Charlou, A. Babarit, and L. Gentaz. A new validated open-source numerical tool for the evaluation of the performance of wind-assisted ship propulsion systems. *Mechanics & Industry*, 24:26, 2023. ISSN 2257-7750. doi: 10.1051/meca/2023026.

T. I. Fossen. *Handbook of Marine Craft Hydrodynamics and Motion Control*. Wiley, Apr. 2011. ISBN 9781119994138. doi: 10.1002/9781119994138.

ITTC. ITTC – Recommended Procedures and Guidelines : 1978 ITTC Performance Prediction Method. Technical report, 2014. URL https://ittc.info/media/4068/75-02-03-014.pdf.

M. Kolodziejski and M. Sosnowski. Review of Wind-Assisted Propulsion Systems in Maritime Transport. *Energies*, 18(4):897, Feb. 2025. ISSN 1996-1073. doi: 10.3390/en18040897.

J. V. Kramer and S. Steen. Sail-induced resistance on a wind-powered cargo ship. *Ocean Engineering*, 261:111688, Oct. 2022. ISSN 0029-8018. doi: 10.1016/j.oceaneng.2022.111688.

L. Marimon Giovannetti, K. Ljungqvist, and S. Werner. Variation of underwater appendages and their effects on wind powered ships. In *7th High Performance Yacht Design Conference 2021*. Curran Associates, Inc., 2021.

R. Okuda, H. Yasukawa, and A. Matsuda. Validation of maneuvering simulations for a KCS at different forward speeds using the 4-DOF MMG method. *Ocean Engineering*, 284:115174, Sept. 2023. ISSN 0029-8018. doi: 10.1016/j.oceaneng.2023.115174.

F. Stern, K. Agdraup, S. Y. Kim, A. C. Hochbaum, K. P. Rhee, F. Quadvlieg, P. Perdon, T. Hino, R. Broglia, and J. Gorski. Experience from SIMMAN 2008 - The First Workshop on Verification and Validation of Ship Maneuvering Simulation Methods. *Journal of Ship Research*, 55(02):135–147, June 2011. ISSN 1542-0604. doi: 10.5957/jsr.2011.55.2.135.

F. Tillig and J. W. Ringsberg. Design, operation and analysis of wind-assisted cargo ships. *Ocean Engineering*, 211:107603, 2020. ISSN 0029-8018. doi: 10.1016/j.oceaneng.2020.107603. URL https://www.sciencedirect.com/science/article/pii/S0029801820306077.

N. J. van der Kolk, I. Akkerman, J. A. Keuning, and R. H. M. Huijsmans. Low-aspect ratio appendages for wind-assisted ships. *Journal of Marine Science and Technology*, 26(4):1126–1143, Feb. 2021. ISSN 1437-8213. doi: 10.1007/s00773-020-00777-8.

H. Yasukawa and Y. Yoshimura. Introduction of MMG standard method for ship maneuvering predictions. *Journal of Marine Science and Technology*, 20(1):37–52, Nov. 2014. ISSN 1437-8213. doi: 10.1007/s00773-014-0293-y.